# Flexible Assembled Metamaterials for Infrared and Microwave Camouflage

Namkyu Lee[a], Joon-Soo Lim[b], Injoong Chang[b], Hyung Mo Bae[b], Juyeong Nam[b], Hyung Hee Cho[b,*]

a. IBI-4, Forschungszentrum Juelich GmbH, 52425 Jülich, Germany

b. Department of Mechanical Engineering, Yonsei University, 50 Yonsei-ro, Seodaemun-gu, Seoul 13722, Korea

* Corresponding author

Tel.: +82 2 2123 2828

Fax: +82 2 312 2159

E-mail: hhcho@yonsei.ac.kr

## Abstract

Light, heat, and waves in electromagnetic energy are the foundation for the advancement of human being. Camouflage materials based on metamaterials are used to excel the performance limits by manipulating the electromagnetic energy. However, multispectral camouflage materials with flexibility are difficult to fabricate because required radiative properties in each spectral regime are different, and largely different scales of the unit cell in a single structure. We propose flexible assembled metamaterials (FAM) by assembling the flexible IR emitter and flexible microwave absorber. We adopt the intermediate layer to assemble the IR emitter and the microwave absorber, leading to securing the selective emission in infrared wave measured by FT-IR measurement and broadening the wavelength of microwave absorption. We calculate the energy dissipation of accumulated energy due to the lowering the radiative energy in the IR regime similar to that of conventional camouflage materials. The wavelength having required absorption (>0.9) for microwave camouflage is wider 2–12 GHz than the conventional microwave absorber. FAM demonstrate multispectral camouflage performances through the decrease in the contrast radiant intensity for IR wave by 75% and the radar cross section for microwave by 99% compared to reference surfaces.

**Keywords**:

*Flexible Assembled Metamaterials; Multispectral Camouflage; Energy dissipation; IR Camouflage; Microwave Camouflage;*

## 1. Introduction

Light, heat, and waves in electromagnetic energy are the foundation for thriving the human being's advancement by utilizing the intrinsic properties of nature materials such as absorption, reflection, scattering and emission[1]. However, due to the performance limits of conventional materials, various needs in building energy management[2,3], packing technology[4,5], safety[6] and military applications[7] cannot be satisfied sufficiently, which leads to developing advanced materials having the engineered properties depending on their missions[8]. The camouflage platform with metamaterials to manipulate electromagnetic energy efficiently is one of the solutions to satisfy the needs in energy[9,10], military[11–15] and space applications[16]. Hence, many researchers have developed several camouflage platforms with metamaterials[17,18], such as metal-dielectric-metal (MDM) structure[19,20], photonic crystal[21], multi-layers[22,23], and novel materials[24–27] to control the electromagnetic energy for breaking the limits of conventional applications[28,29].

There are two camouflage mechanisms: reduction in the reflection or the emission from the target against the detector at the specific wavelength. In reducing the reflected wave from the target such as the microwave[30,31], metamaterials for microwave camouflage match the impedance with the medium and consume the incident wave through the energy dissipation in the structure, inducing the unity of absorptivity. Otherwise, when the detector measures the emitted wave from the target in IR wave, the emissivity (absorptivity) in the detected band should be zero; it means the unity reflectivity on the surface contrary to the metamaterials for microwave camouflage. These different mechanisms make the multispectral camouflage difficult because camouflage materials should satisfy both the zero and the unity absorptivity in the different spectral regimes in the same structure. Furthermore, blocking the signal from the target can induce energy accumulation based on the energy conservation law[32], meaning that we also need to consider the energy dissipation through the undetected spectrum to prevent the unwanted energy accumulation in the structure[33].

Therefore, there have been several studies on metamaterials for camouflage with a specific property of the unity absorptivity for microwave[30,31,34] or reflectivity for IR wave[33,35–37].

However, only a few studies of the multispectral metamaterials have been conducted[38,39] since they should solve the issue of size difference depending on the target wavelength. In metamaterials, the operating wavelength is proportional to the unit cell size. This requires that they contain various unit-cell sizes in the same structure to cover the multispectral wavelength range such as microwave (O ~ cm) and IR wave (O ~ μm)[40], which makes the fabrication difficult. Researchers have applied the intermediate layer[19], multi-thin layers[22] or the different electromagnetic properties of the material[41] to cover the multispectral camouflage for overcoming this difficulty. However, the issue of the material flexibility is still remained because the shape of the surface in a real application is highly arbitrary, making it difficult for brittle materials to be applied on the surface directly.

In order to make the flexible multispectral metamaterials, the change in polymers of composed materials is one of the options since they can make a thick dielectric layer (O ~ mm) easily to match the impedance with the medium in the microwave frequency. However, it is inappropriate as a dielectric layer in IR camouflage materials because it induces the multi-resonance, making their manipulation in the IR regime difficult[37]. It implies that the flexible IR camouflage material with the dielectric layer not to induce multi-resonances should be assembled to the flexible microwave absorber separately. Disconnecting the brittle layer as the engineering solution to reduce the mechanical stress leads to the flexible structure for arbitrary surfaces[42] similar to the conventional IR camouflage materials. Based on these materials, when we change the function of flexible IR camouflage materials in having IR camouflage and microwave transparency, then multispectral camouflage materials can be realized by assembling each IR and microwave camouflage material.

We propose the flexible assembled metamaterials (FAM) to realize the multi-spectral camouflage in the single structure. With the intermediate layer, we fabricated FAM by assembling the flexible IR emitter (FIRE)

and microwave absorber (FMWA). FIRE reduces the stress concentration and lets the microwave penetrate into FMWA by disconnecting the metal ground and dielectric layer. FIRE has the same mechanism and performance as conventional camouflage materials based on the simulation and analytical approach. FMWA enhances the bandwidth of high absorptivity (> 0.9) in the S (2-4 GHz), C (4-8 GHz) and X (8-12 GHz) in the single structure due to the intermediate layer. We simulated the multi-spectral camouflage performance on the arbitrary structures in terms of the contrast radiant intensity (CRI) in the IR and the radar cross section (RCS) in the microwave. We confirm that FAM has the comparable IR camouflage performance and the surpassing microwave camouflage performance than the hierarchical metamaterials[19].

## 2. Results and Discussion

### 2.1. Strategy of flexible assembled metamaterials for both camouflages in IR and microwave

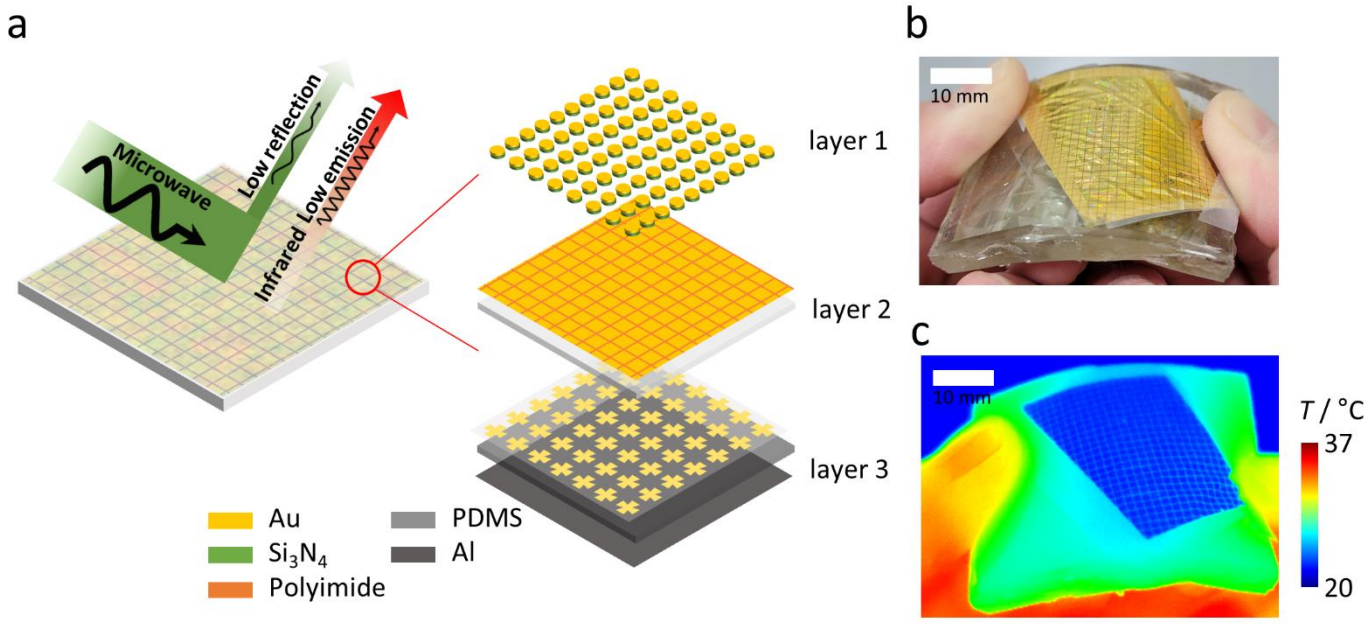


**Figure 1**. Overview of flexible assembled materials (FAM) for both infrared (IR) and microwave camouflage with assembled structures consisting of flexible IR emitter (FIRE) and microwave absorber (FMWA). (a) Schematic of incoming and outgoing microwave and IR radiation including structures of FAM integrated by FIRE (layers 1+2) and FMWA (layer 2+3). Layer 2 is for dual purposes: it acts as a metal ground for a flexible IR emitter in FIRE, and it acts as a low-pass filter to increase the broadband absorption in FMWA. (b,c) Optical and infrared images of fabricated materials presenting the material flexibility and IR camouflage performance. Scale bar in (b,c) is 10 mm.

Metamaterials for multispectral camouflage have specific target wavelengths such as IR (3–5 μm and 8–12 μm) and microwave (3–10 cm), which induces the difference in unit cell size (IR ~ O (μm), microwave ~ O (cm)) in the order of 3. It implies that the fabrication is one of the complex problems to integrate the multispectral camouflage materials. The other problem is the interaction of each component to other target wavelengths. Typically, the metal (Au) has the unity reflectivity in IR and microwave, which causes the total reflection of other target wavelengths. However, the metal ground in the MDM structure induces the total reflection of incoming and outgoing IR and microwave even though we require the operation of each MDM

structure separately. Millions of IR emitters can be located on the general metal pattern for microwaves due to the large size difference of unit cells. These patterns also act as low pass filters, only allowing wavelengths below the specific wavelength to pass through. Therefore, the multispectral metamaterials can be achieved when the intermediate layer with dual purposes is fabricated.

Figure 1 shows the overview of FAM. As shown in Fig. 1(a), there are three parts: layer 1 for IR selective emission, layer 3 for microwave selective absorption, and layer 2 for both IR and microwave. On the one hand, layer 2 as FIRE acts as the metal ground because of the size of the unit cell (1.3 cm × 1.3 cm) with a pitch of 1.4 cm, which implies that millions of unit cells of the IR emitter lie on the metal pattern of layer 2. On the other hand, layer 2, as FMWA, act as the low pass filter targeting unit cell size below the minimum wavelength of X-band covering 2.5 cm–3.7 cm (8 GHz–12 GHz). Our target wavelength of microwave absorber was S (7.5 cm–15 cm, 2 GHz–4 GHz), C (3.7 cm–7.5 cm, 4 GHz–8 GHz) and X band, which are widely used to chase the target[43]. FAM can cover both camouflage performance in IR and microwave due to layer 2.

In order to demonstrate the materials flexibility and IR camouflage simultaneously, Figs. 1(b) and (c) show the optical and infrared images of FAM with bending the structure. Figure 1(b) shows the bending structure as well as the IR camouflage performance can be achieved, as shown in Fig. 1(c) despite the small gap between unit cells having a minute impact. Moreover, we recognize that FIRE is successful in operating the low IR emission for IR camouflage in the detected wavelengths of the IR camera (7.5 μm–14 μm) as expected.

## 2.2. Optical characteristics of flexible assembled metamaterials

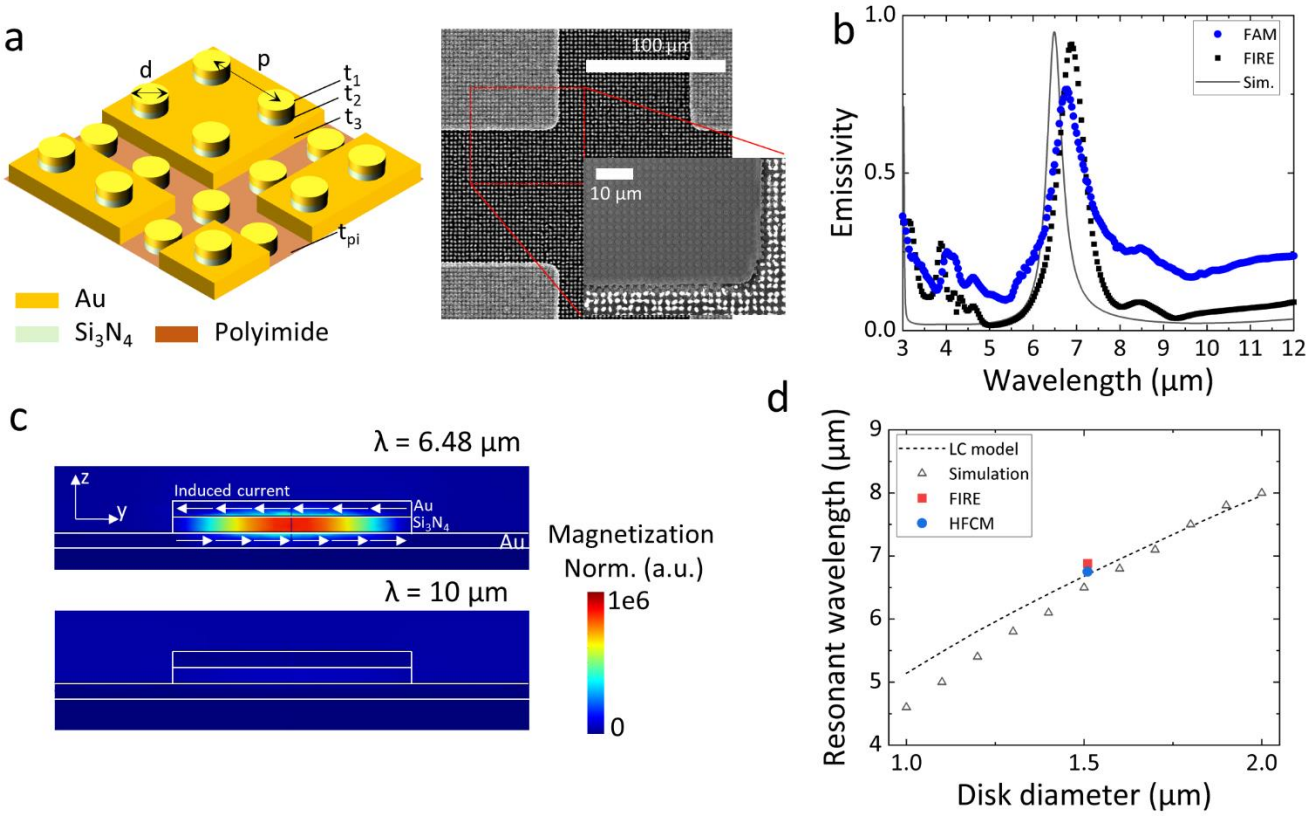


**Figure 2**. Flexible IR emitter (FIRE) in FAM controlling a thermal signature. (a) Unit-cell structure of FIRE in FAM. Thicknesses of $t_1$, $t_2$ and $t_3$ were fixed at 100 nm. Diameter d, and pitch p were 1.51 μm and 3 μm, respectively, influencing the resonance frequency in IR band for efficient energy dissipation. (b) Measured and simulated spectral emissivity of FIRE and FAM. Scattered data represent the experiment and line data express the simulation. (c) Electromagnetic behavior in the unit cell of FIRE in FAM at the resonant wavelength of 6.48 μm and at the non-resonant wavelength of 10 μm. (d) Resonant wavelength along the diameter of FAM unit cell. Based on the LC model and simulation, the resonant wavelength was estimated. FIRE and FAM lie on the estimated line.

Figure 2(a) shows the schematic of FIRE in FAM whicn controls a thermal signature. FIRE for FAM consisted of four parts: 1) polyimide layer, 2) discrete metal ground, 3) dielectric disk and 4) metal disk. Polyimide is widely used as a substrate for flexible materials because it has high mechanical and chemical resistance and ease of the fabrication through the spin coating from a liquid state of material[44], proving the general usage without the consideration of the distortion of material. Its thickness ($t_{pi}$) is 13 μm with 3000 rpm

for 30 s. Discrete metal grounds–the important part–were located on the polyimide. As mentioned above, the whole-covered metal grounds blocked the microwave completely, preventing the ingoing and outgoing wave from reaching microwave absorber. Thus, we separated the gap (100 μm) between metal grounds with the thickness ($t_3$) of 100 nm, inducing the blocked IR wave and penetrating microwave. The material of metal ground was Au widely used in a microfabrication.

There are two ways to fabricate flexible materials: 1) using flexible polymers in each component and 2) changing structures to reduce the mechanical stress. It is difficult to use IR camouflage materials in case of flexible polymers because the dielectric layer has lots of lattice resonance in IR band which induces unwanted resonances[37,45]. Hence, the structure of IR camouflage materials should be changed, such as disconnecting the brittle part to reduce the mechanical stress[42]. As a dielectric layer, silicon nitride ($Si_3N_4$) was adopted for FAM. The transparent material, such as ZnS[46] or $Al_2O_3$[47], is generally used for IR camouflage materials because its lattice vibration in IR band induces additional resonances. However, if the thickness is sufficiently small to ignore the effect of dielectric layer, we can use the silicon-based material because its deposition has been widely used in the micro-nano fabrication. Therefore, we chose silicon nitride with the thickness ($t_2$) of 100 nm, which is sufficiently transparent to be use in IR camouflage materials. The diameter (d) and the pitch (p) of disk were 1.51 μm and 3 μm, respectively. The thickness of metal and dielectric disk ($t_1$) was 100 nm each. Based on this strategy, scanned electron microscope (SEM) image in Fig. 2(a) shows that the designed unit cell is constructed successfully.

Figure 2(b) shows the spectral emissivity with FAM, FIRE, and simulation. FIRE (Fig. 2(b)) was fabricated with Au surface without discrete metal grounds. FAM has a similar spectral emissivity in 3–12 μm as FIRE. The peak emissivity of FIRE was 0.91 at 6.88 μm and that of FAM was 0.76 at 6.75 μm. This difference is caused by the gap between metal ground in FAM. As mentioned above, Au as a metal ground covered 86% of whole area. Unit cell of FIRE cannot operate without metal ground because the magnetic field does not occur

in the dielectric layer. The 86% of peak emissivity of FIRE was 0.78 meaning that unit cells to induce the selective emission in IR regime operate successfully except on the gap. The low emissivity in 8–12 μm increased owing to the gap. Considering the FIRE averaged emissivity of 0.1 in 8–12 μm, the averaged emissivity was 0.23 considered by the area ratio between the metal ground and the gap. This value is close to the measured emissivity of 0.22 in 8-12 μm. We believe that the polyimide thick film (> 10 μm) has the unity emissivity in IR regime, which increases the emissivity[48]. From these outcomes, the fabricated FIRE in FAM operates sufficiently to make the selective emission for the reduced radiative energy in detected band (3–5 μm and 8–12 μm) and the energy dissipation of accumulated energy through the undetected band (5–8 μm) as much as possible.

We simulated the magnetic field in the cross-sectional surface to analyze the electromagnetic mechanism in FIRE. Figure 2(b) shows that the simulated result is similar to experimental results implying that we can use the simulated result to understand the electromagnetic behavior in FIRE. Figure 2(c) shows the norm of magnetization in the unit cell of FIRE. A localized magnetic resonance is generated at the resonance of 6.48 μm. However, there was no magnetization in a dielectric layer at the wavelength of 10 μm. It means that the induced magnetic resonance in FIRE causes the selective emission to the undetected band, and FIRE at the detected band acts as the low emissivity material for IR camouflage.

We compared the resonant wavelength with the simulation and analytical approach to verify whether the same electromagnetic behavior is seen between FIRE solely and FAM. If the resonant wavelength lies on the interpolated line, the electromagnetic behavior of FIRE and FAM is the same from the simulation and analytical approach. As shown in Fig. 2(d), the LC model and simulation agree well with experimental results in FIRE and FAM. These results show that FIRE and FAM have the same mechanism for inducing the selective emission for IR camouflage. Additionally, the LC model of FIRE also predicts the resonance wavelength for FAM with different wavelengths, meaning that FAM can expand its applications for the different wavelength.

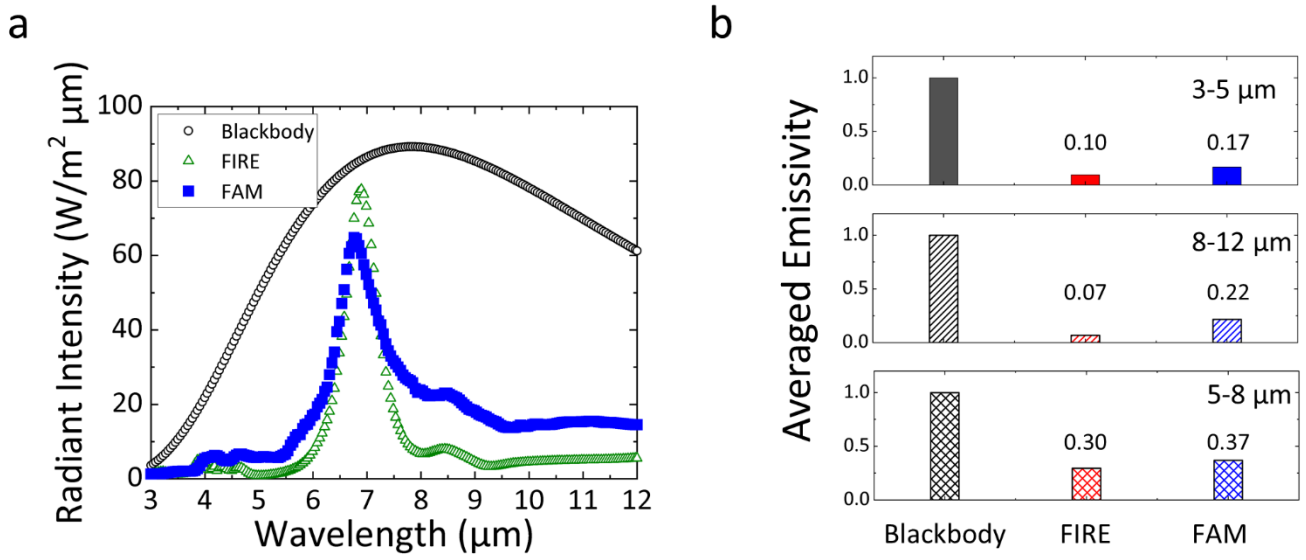


**Figure 3**. Radiant intensity representing the energy dissipation and camouflage performance. (a) The spectral radiant intensity of blackbody, FIRE and FAM. A blackbody is the maximum radiant intensity. (b) Comparison of radiative flux in detected bands and undetected bands. The detected bands are 3–5 μm and 8–12 μm. The undetected band is 5–8 μm requiring a higher radiative flux. In the detected bands, the lower value is better to hide the target from the detector. In the undetected bands, the higher value is better to dissipate more energy into the environment.

We evaluated the radiative energy in each band based on these characteristics. The radiative energy in the detected band (3–5 μm and 8–12 μm) should decrease, as mentioned above. Such energy in the undetected band (5–8 μm) should increase because the reduced radiative energy can induce thermal instability due to the energy accumulation inside the system. The radiant intensity for the radiative energy in the detected and undetected bands is calculated as follows[49]:

$$E_{b\lambda}(\lambda, T) = \frac{2\pi h c_0^2}{\lambda^5 \left[\exp[\frac{hc_0/k}{\lambda T} - 1]\right]} \quad (1)$$

where h, $c_0$, k, and T represent Planck's constant, the speed of light in vacuum, Boltzmann's constant, and the temperature, respectively. After calculating Eq. (1), we integrated the radiant intensity for the radiative energy, as follow:

$$E_{\lambda_1-\lambda_2}(T) = \int_{\lambda_1}^{\lambda_2} \varepsilon(\lambda, T)\, E_{b\lambda}(\lambda, T)\, d\lambda \cong \sum \varepsilon(\lambda, T)\, E_{b\lambda}(\lambda, T)\Delta\lambda \quad (2)$$

where ε represents the measured emissivity of materials. $\lambda_1$ and $\lambda_2$ denote the minimum and maximum bands, respectively. Figure 3(a) shows the radiant intensity calculated using Eq. (1). The temperature was fixed at 370 K originated from the total temperature in Mach number = 1.5 at the altitude of 5000 m. We evaluated the averaged emissivity to compare the camouflage performance, as shown in Fig. 3(b). The averaged emissivity of FIRE was 0.10 and 0.07 in 3–5 μm and 8–12 μm detected bands, respectively. The average emissivity of FAM was 0.17 and 0.22 in 3–5 μm and 8–12 μm detected bands, respectively. The averaged emissivity of FAM is larger than the FIRE because the polyimide backside of metal grounds induces the higher emissivity as mentioned above. However, Fig. 1(d) shows that FAM leads to the IR camouflage against the IR detector meaning that the averaged emissivity is sufficient to hide the target. Additionally, the microwave can penetrate the microwave absorber through the gap between the metal ground for microwave camouflage, contrary to the FIRE solely, which reflects the entire microwave. The other important function is energy dissipation in the undetected band because the IR camouflage material should compensate for the reduced radiative energy in the detected band. The averaged emissivity of FIRE and FAM was 0.30 and 0.37, respectively, which is 23% larger than the FIRE. It means that the energy dissipation in undetected bands can be compensated the higher emissivity in the detected band by considering the camouflage performance factor[33].

## 2.3. Microwave absorption of FAM

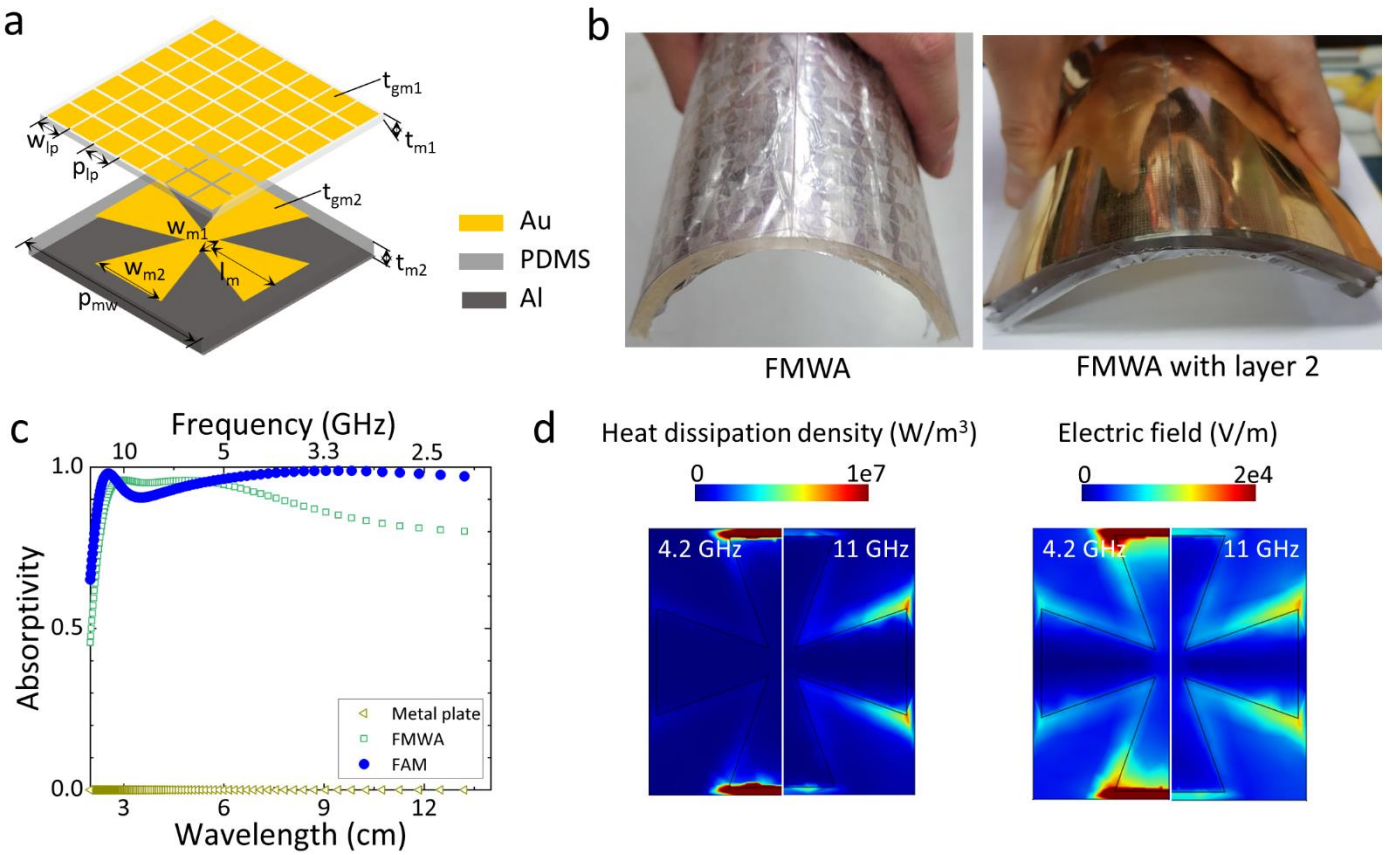


**Figure 4**. FMWA regulates the microwave reflection. (a) Schematic of the unit-cell of FMWA in FAM with a pitch ($p_{mw}$) of 10 mm. Thickness of $t_{gm1}$ and $t_{m1}$ in layer 2 are 200 nm and 4 mm determined from the parametric study. Width and pitch of metal patch are 1.3 mm and 1.4 mm, respectively. In layer 3, thicknesses of $t_{gm2}$ and $t_{m2}$ are 16 nm and 5 mm calculated from the parametric study. Geometrical values of $w_{m1}$, $w_{m2}$ and $l_m$ are 2, 1 and 4.2 mm, respectively. (b) Image of FMWA and FMWA with layer 2 for confirming the material flexibility. (c) Microwave absorption along metal plate, FMWA and FAM. (d) Electromagnetic loss mechanism of FMWA at 4.2 GHz and 11 GHz.

Figure 4(a) shows the schematic of the unit-cell of FMWA in FAM. There are two parts: 1) the upper part (layer 2), composed of square metal patterns (Au) and the dielectric layer (PDMS). 2) lower part (layer 3) consisting of cross-ribbon patterns (Au), the dielectric layer (PDMS), and metal ground (Al). We investigated the parametric effect on microwave absorption to determine the geometrical factors for FMWA in FAM. There are two key factors of the broadband absorption covering S (2-4 GHz, 15 – 7.5 cm), C (4-8 GHz, 7.5 – 3.8 cm)

and X (8-12 GHz, 3.8 – 2.5 cm) bands. The one thing is the thicknesses in dielectric layers ($t_{m1}$, $t_{m2}$) of layer 2 and 3. Figure S3 shows that the thickness of the dielectric layer critically affects the absorptivity. A threshold value in the microwave absorption was 10 dB, the same as the absorptivity of 0.9. To satisfy this criterion, $t_{m1}$ and $t_{m2}$ should be 5 mm and 4 mm, respectively. The other thing is the sheet resistance of resistive pattern on the top surface. Figure S4 shows the effect of absorptivity in microwave based on the sheet resistance. The sheet resistance should be between 20 ohm/sq and 30 ohm/sq to obtain the microwave absorptivity of more than 0.9 because the higher resistance is easier to achieve the higher absorptivity in the target frequency. Based on these results, we conclude that 30 ohm/sq is the best value to achieve the broadband and high absorption for S, C and X bands. A detailed description of the simulation is presented in supporting information.

However, it is difficult to achieve more than 10 ohm/sq in a metal owing to significantly large conductivity. We can use conductive ceramic having a high resistivity such as ITO, however, it is too brittle to bend. Hence, we should choose the metal that is ductile in the ambient temperature. Typically, the electrical conductivity is confined by the thickness of thin film below the mean free path of material[50], meaning that we can control the sheet resistance to decrease the thickness. As shown in Fig. S5, the metal thickness below 20 nm affects the increment of sheet resistance. We chose 14 nm of thickness, which is 30 ohm/sq. Figure 4(b) shows the images to verify the material flexibility despite the total thickness of 9.2 mm.

Figure 4(c) shows that FMWA and FAM can cover the X-band sufficiently when the metal plate of copper is the reference material having zero absorption in the microwave regime. FAM has high absorption in the S and C bands, unlike FMWA, implying that the intermediate layer helps the additional absorption. We compared the heat dissipation density and electric field with the numerical simulation simultaneously to investigate the reason for microwave absorption in S, C and X bands because the absorbed wave in the material converts into the form of thermal energy. As shown in Fig. 4(d), the heat dissipation at X band (11 GHz) happens around the edge of the metal pattern owing to the concentration of the electric field. In the case of the

C band (4.2 GHz), the heat dissipation density occurs between a gap of metal patterns. By comparing Figs. 4(c) and (d), we conclude that the additional heat dissipation between the gaps in FAM induces the high absorption in S and C band compared to FWMA in Fig. S2. It means that the intermediate layer in FAM is helpful in increasing microwave absorption.

## 2.4. Camouflage performance of flexible assembled metamaterials on applications

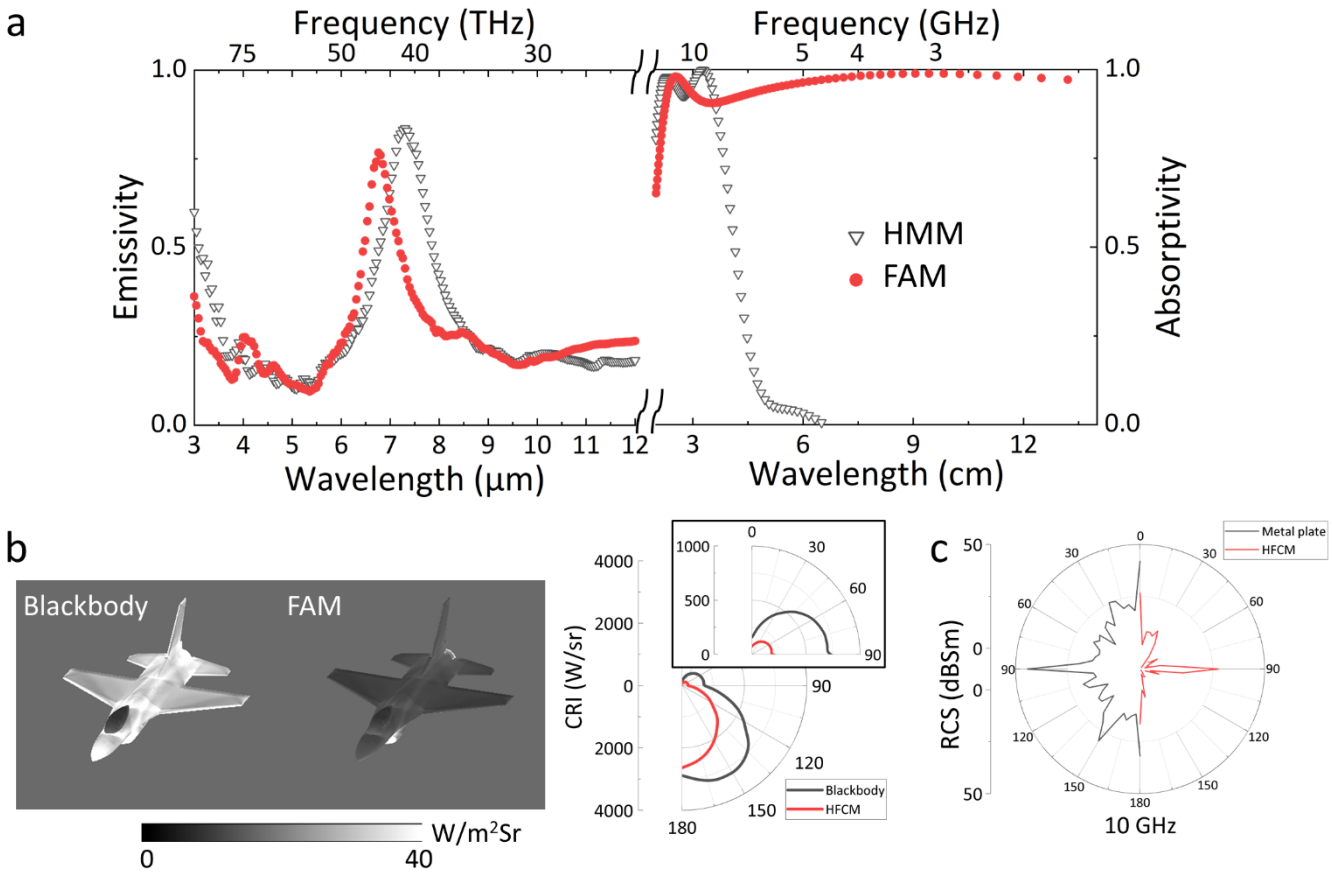


**Figure 5.** (a) Comparison of IR emissivity and microwave absorption between HMM and FAM. (b) Simulated IR image and contrast radiant intensity of modelled aircraft along blackbody and FAM, representing IR camouflage performance in 8–12 μm band. (c) Simulated radar cross-section at 10 GHz along the metal plate and FAM, which explains MW camouflage performance.

We compared the spectral emissivity and absorptivity between the hierarchical metamaterials (HMM)[19] and FAM to check the camouflage performance. Figure 5(a) shows the spectral emissivity in the IR band and the spectral absorptivity in the microwave. As shown in Fig. 5(a), we find that the spectral emissivity in the IR band shows a similar performance between HMM and FAM. Particularly, the spectral emissivity of the previous work and FAM in detected bands (3–5 μm and 8–12 μm) is approximately identical, meaning that FAM has the same performance in the IR band and in HMM. Interestingly, the microwave absorption of FAM

is wider than HMM. The previous work only covered the X–band, whose performance is limited to the specific purpose. However, FAM covers the S, C, and X bands, which can be used against broadband microwave detection. Furthermore, HMM cannot provide material flexibility, which means that material is only utilized as a tile type having a limitation on the curved surface. However, FAM can be used on arbitrary surfaces, extending applications without considering the surface shape.

Additionally, we evaluated FAM of the IR and microwave camouflage performance in actual applications. The aircraft-like CAD file shown in Fig. 5(b) was chosen to evaluate the camouflage performance. We used the TATIhermIR v.13 for IR camouflage, a commercial program widely used as the radiative signal based on the IR surface emissivity and atmospheric condition[51]. Figure 5(b) shows the IR image with the background from the isotropic view. The background is the sky, which induces low radiative energy owing to low temperature. As shown in Fig. 5(b), the contrast between the background and the aircraft covered with FAM is significantly less than blackbody implying the unity emissivity. It means that FAM qualitatively shows sufficient IR camouflage performance. We evaluated the contrast intensity ratio (CRI) by considering the IR signal of the background and the target area simultaneously to quantify this qualitative IR camouflage performance. Figure 5(b) shows that the CRI of FAM is 75% decreased by the blackbody at 90°. This decrease in CRI can make the half of susceptibility with the blackbody by considering the lock-on and lethal range[51]. It shows that FAM can provide sufficient IR camouflage performance according to the qualitative and quantitative evaluation.

We also evaluated the RCS using the measured data of microwave absorptivity. We used FEKO v 14.0, a commercial program used to analyze the ray tracing of a large-scale structure[19]. The RLGO model is used for RCS from the target. The reference surface was a perfect conductor surface (PCS) with the unity reflectivity. As shown in Fig. 5(c), the graph represents the RCS at 10 GHz depending on the metal plate and FAM on the surface. It shows that the FAM can reduce the RCS dramatically than the metal plate. We can obtain, based on

the quantitative value of RCS, at most -31 dB, which is converted into 0.06% of RCS on the metal plate. These results, such as CRI and RCS, show that FAM can sufficiently satisfy both camouflage performance, i.e., reducing the emission of IR signal in the detected band and absorbing the microwave signal from the detector. Note that the angle dependence of material is included indirectly as a dielectric layer with the thickness and material properties. The detailed description of angle dependence is written in the supporting information. In conclusion, based on these results, we confirm that FAM have the IR and microwave camouflage performance simultaneously on the actual application.

## 3. Conclusion

We propose FAM for multi-spectral camouflage such infrared and microwave. We adopted the intermediate layer to assemble FIRE and FMWA for both purposes–the metal ground in FIRE and the low pass filter in FMWA. The spectral emissivity of FAM is similar to that of the FIRE despite the discrete metal ground of FAM. Moreover, we note based on the simulation and LC circuit model that the electromagnetic behavior as a magnetic resonance in the IR band has the same mechanism between the FIRE and FAM. In the case of radiative energy as the IR camouflage performance, even though the emissivity of FAM in detected bands (3–5 μm and 8–12 μm) is larger than the FIRE, the energy dissipation of FAM through the undetected band (5–8 μm) is also larger than the FIRE. It means that the larger energy dissipation of FAM through the undetected band can compensate for larger radiative energy in the detected band than in FIRE. In the microwave absorption, the absorptivity above 0.9 of FAM covers from 2 GHz to 12 GHz such as S (2–4 GHz), C (4–8 GHz) and X (8–12 GHz). The designed pattern of FAM targets the X band. However, the intermediate layer induces the additional loss mechanisms compared to the FWMA affecting the S and C bands making the broadband absorption in the microwave possible. We evaluated the IR and microwave camouflage performance for quantitative comparison based on the measured emissivity and absorptivity depending on the wavelength. The spectral emissivity of HMM and FAM in the IR band is identical. The microwave absorptivity of FAM is significantly wider than HMM, which can only cover in the X band. It means that FAM has a broader camouflage performance in the microwave and material flexibility which can be applied to an arbitrary surface. Additionally, we evaluated CRI for IR camouflage, considering the signal difference between the target and background. CRI with FAM decreased by 75% than the blackbody surface, which decreases the half of susceptibility of the target than the blackbody. Moreover, we also calculated the RCS covered by FAM. The results show that 99% of the microwave reflection can be reduced by the FAM surface. Furthermore, these outcomes demonstrate that FAM has abilities for both camouflage in IR and microwave. We expect that FAM

would provide a clue for designing the multi-spectral control with material flexibility and spread various applications such as energy conversion, space, and military field.

## 4. Experimental Section

### Fabrication of flexible infrared emitter

The fabrication was based on the silicon wafer with a thickness of 500 nm. The cleaning process followed three steps: acetone, ethanol, and buffered-oxide etchant (BOE) with 10 min each, which removed organic matters from the wafer. After that, the VTEC 1388—liquid polyimide—was coated with 3000 rpm that induced the thickness of 13 μm; it was used as a substrate and separate FIRE from the wafer. Photoresist patterns were fabricated on the polyimide-deposited wafer as a low pass filter of FMWA and a metal ground of FIRE. The photoresist (AZ5214E, Microchemicals GmbH, Germany) was coated for patterns using a spin coater (3000 rpm, 30 s). The mask aligner (MA6, Karl SÜSS MICROTEC SE, Germany) induced patterns on the photoresist-deposited surface. Furthermore, the electron beam (E-beam) evaporator (ULVAC, Japan) was used to deposit Au/Ti layers with 100/10 nm, respectively. Ti was used as an adhesive layer which did not affect the FIRE performance[19,28,33,37]. The silicon nitride for a dielectric layer and Au/Ti layers for metal patterns were deposited by plasma enhanced chemical vapor deposition (PECVD, Plasma Therm 790 Series, Plasma Therm USA) and E-beam evaporator after lifting off the photoresist, respectively. Photoresist patterns were fabricated on metal (Au)-dielectric ($Si_3N_4$)-metal (Au) layers for disk structure by controlling the magnitude of exposure dose (50 – 200 mJ/cm$^2$) by varying the diameter of the unit cell. After that, inductively coupled plasma (ICP, Oxford etcher, Oxford Instruments) was used for etching the metal and dielectric layer except for metal ground. Moreover, we used a plasma asher of 100 W for 5 min to remove the remained photoresist.

### Fabrication of flexible microwave absorber

The FMWA consisted of two parts such, one of which was a microwave absorber (MWA) to absorb the microwave primarily. MWA was composed of metal ground, a spacer of a dielectric material, and a metal pattern. The aluminum adhesive tape was chosen as a metal ground because of sufficiently large electrical

conductivity that would reflect the entire incident wave; moreover, it has material flexibility with easy machinability. Polydimethylsiloxane (PDMS) of 5 mm consisted of Sylgard 184 and the curing agent with the mass ratio of 10:1. The curing process was conducted for 10 min at 115°C was with 10 minutes because of the thermosetting material of PDMS. The thickness of PDMS was controlled by the size of the frame. The polyethylene terephthalate (PET) film with a metal pattern was attached to the PDMS spacer. The metal pattern with 14 nm thickness was deposited with a sputter whose value matched with the sheet resistance of 30 Ohm/sq.

**Attachment between FIRE and FMWA**

After finishing the fabrication of FIRE on the silicon substrate, we cut the FIRE 7 cm by 7 cm, which size is the biggest size to obtain from the substrate securely. Then, we attach the scotch tape along the cutting line as small as possible. Then when we pull the scotch tape from the substrate, then we can get the FIRE with 7 cm by 7 cm. After that, we can attach the FIRE on the FMWA with liquid PDMS as an adhesive layer.

**Measurement of infrared emissivity**

Fourier transform infrared spectroscopy (FT-IR, Bruker Corp.) was used to quantify the spectral emissivity. A phase difference of a signal was analyzed using the beam splitter (KBr). The measurement range of FT-IR was 1.3 μm–27 μm. The reflectivity was measured using the accessory of FT-IR (Bruker A513). Furthermore, the reflectivity was calculated using the following equation: $\rho(\lambda) = S_{sample}(\lambda,T) / S_{reference}(\lambda,T)$. The reference surface was thick gold (200 nm), whose reflectivity can be assumed to be 1. Based on the Kirchhoff's law, the reflectivity ($\rho(\lambda)$) was converted into the absorptivity (emissivity) with the following expression: $\alpha(\lambda) = \varepsilon(\lambda) = 1 - \rho(\lambda)$. The temperature was the ambient temperature during the measurement controlled by the air-conditioning system in the laboratory. The size of the sample was 1.3 cm × 1.3 cm.

**Measurement of microwave absorptivity**

The vector network analyzer (VectorStar MS 4642B VNA) was used to measure the microwave absorptivity. The network analyzer could measure from 2 GHz to 18 GHz with K connectors (Anritsu), which was used to measure the S-parameter of the test specimen[19]. Two Vivaldi antennas were used for the plane wave experiment owing to a polarization with respect to the shape of the antenna. One of the antennas emitted the microwave signal, and the other received the signal from the reflected wave. We evaluated the reflection coefficient based on the signal ratio between two antennas. The length between the test specimen and antennas satisfied the far-field condition owing to the S-parameter calculation. The specimen was installed in the periphery of wave absorbing material to diminish the effect of arbitrarily reflected waves. A copper plate with 15 cm × 15 cm size was used as a reference plate, whose reflectivity was assumed to be 1. The test specimen with 14 cm × 14 cm size was made from the unit cell of FAM with a size of 7 cm × 7 cm.

**Thermographic and visible measurement**

An IR camera in the 7.5 μm – 14 μm range (A655sc, FLIR Systems, Wilsonville, OR, US) was used for measuring the IR image to observe the performance of IR camouflage. The temperature of the specimen was assumed to be the ambient temperature controlled by the air-conditioning system. The processed emissivity of 0.95 was considered a default for the IR camera to compare the difference in infrared radiation from a specimen. The visible image was measured using the camera with the following specifications: 12 megapixels and f/2.4 aperture. It demonstrated the material flexibility of FAM.

## Author Information


### Corresponding Author

*E-mail: hhcho@yonsei.ac.kr


## Author contributions

N. L., and H. H. C. designed the overall strategy. N. L. and J.-S. L. fabricated the specimen and measured the spectral emissivity through FT-IR and VNR facility. N. L. and I. C. performed the numerical simulation for revealing the electromagnetic behaviors. J.-S. L. and H. B. captured the visible and infrared images to evaluate the camouflage performance. N. L. and J. N. simulated the CRI and RCS calculation with FAM. All the authors analyzed the data. N. L. and H. H. C. wrote and supervise the manuscript.

## Acknowledgements


This work was supported by the Aerospace Low Observable Technology Laboratory Program of the Defense Acquisition Program Administration and the Agency for Defense Development of the Republic of Korea.

## References


[1] S. Dou, H. Xu, J. Zhao, K. Zhang, N. Li, Y. Lin, L. Pan, Y. Li, *Adv. Mater.* **2021**, *33*, e2000697.

[2] I. Hernández-Pérez, G. Álvarez, J. Xamán, I. Zavala-Guillén, J. Arce, E. Simá, *Energy Buildings* **2014**, *80*, 81.

[3] C. Zhang, O. B. Kazanci, R. Levinson, P. Heiselberg, B. W. Olesen, G. Chiesa, B. Sodagar, Z. Ai, S. Selkowitz, M. Zinzi, A. Mahdavi, H. Teufl, M. Kolokotroni, A. Salvati, E. Bozonnet, F. Chtioui, P. Salagnac, R. Rahif, S. Attia, V. Lemort, E. Elnagar, H. Breesch, A. Sengupta, L. L. Wang, D. Qi, P. Stern, N. Yoon, D.-I. Bogatu, R. F. Rupp, T. Arghand, S. Javed, J. Akander, A. Hayati, M. Cehlin, S. Sayadi, S. Forghani, H. Zhang, E. Arens, G. Zhang, *Energy Buildings* **2021**, *251*, 111312.

[4] S. P. Singh, G. Burgess, J. Singh, *Packag. Technol. Sci.* **2008**, *21*, 25.

[5] S. Singh, K. K. Gaikwad, Y. S. Lee, *Environ. Chem. Lett.* **2018**, *16*, 845.

[6] A.-L. Davesne, T. Bensabath, J. Sarazin, S. Bellayer, F. Parent, F. Samyn, M. Jimenez, F. Sanchette, S. Bourbigot, *ACS Appl. Polym. Mater.* **2020**, *2*, 2880.

[7] L.V. Wake, R.F. Brady, *Formulating infrared coatings for defence applications, Research report,* **1993**.

[8] X. Luo, M. Pu, Y. Guo, X. Li, X. Ma, *Adv Photo Res* **2021**, *2*, 2100023.

[9] S. Hong, S. Shin, R. Chen, *Adv. Funct. Mater.* **2020**, *30*, 1909788.

[10] A. Lenert, D. M. Bierman, Y. Nam, W. R. Chan, I. Celanović, M. Soljačić, E. N. Wang, *Nat. Nanotechnol.* **2014**, *9*, 126.

[11] L. Li, M. Shi, X. Liu, X. Jin, Y. Cao, Y. Yang, W. Wang, J. Wang, *Adv. Funct. Mater.* **2021**, *31*, 2101381.

[12] J. Lee, H. Sul, Y. Jung, H. Kim, S. Han, J. Choi, J. Shin, D. Kim, J. Jung, S. Hong, S. H. Ko, *Adv. Funct. Mater.* **2020**, *30*, 2003328.

[13] Y. Qu, Q. Li, L. Cai, M. Pan, P. Ghosh, K. Du, M. Qiu, *Light Sci. Appl.* **2018**, *7*, 26.

[14] Y. Zhao, F. Fang, *ACS Appl. Electron. Mater.* **2021**, *3*, 2694.

[15] P. Won, K. K. Kim, H. Kim, J. J. Park, I. Ha, J. Shin, J. Jung, H. Cho, J. Kwon, H. Lee, S. H. Ko, *Adv. Mater.* **2021**, *33*, e2002397.

[16] K. Sun, C. A. Riedel, A. Urbani, M. Simeoni, S. Mengali, M. Zalkovskij, B. Bilenberg, C. H. de Groot, O. L. Muskens, *ACS Photon.* **2018**, *5*, 2280.

[17] Denis G. Baranov, Yuzhe Xiao, Igor A. Nechepurenko, Alex Krasnok, Andrea Alù, Mikhail A. Kats, *Nat. Mater.* **2019**, *18*, 920.

[18] J. Yang, X. Zhang, X. Zhang, L. Wang, W. Feng, Q. Li, *Adv. Mater.* **2021**, *33*, e2004754.

[19] T. Kim, J.-Y. Bae, N. Lee, H. H. Cho, *Adv. Funct. Mater.* **2019**, *29*, 1807319.

[20] N. W. Pech-May, L. Tobias, M. Retsch, *ACS Appl. Mater. Interf.* **2021**, *13*, 1921.

[21] J. Teyssier, S. V. Saenko, D. van der Marel, M. C. Milinkovitch, *Nat. Commun.* **2015**, *6*, 6368.

[22] H. Zhu, Q. Li, C. Tao, Y. Hong, Z. Xu, W. Shen, S. Kaur, P. Ghosh, M. Qiu, *Nat. Commun.* **2021**, *12*, 1805.

[23] H. Liu, C. Wang, G. Chen, Y. Liao, M. Mao, T. Cheng, A. Libanori, X. Xiao, X. Hu, K. Liu, J. Chen, *Nano Energy* **2022**, *93*, 106855.

[24] X. Xie, X. Li, M. Pu, X. Ma, K. Liu, Y. Guo, X. Luo, *Adv. Funct. Mater.* **2018**, *28*, 1706673.

[25] Y. Huang, B. Ma, A. Pattanayak, S. Kaur, M. Qiu, Q. Li, *Laser Photon. Rev.* **2021**, *15*, 2000391.

[26] T. Han, X. Bai, J. T. L. Thong, B. Li, C.-W. Qiu, *Adv. Mater.* **2014**, *26*, 1731.

[27] Y. Li, C. Xiong, H. Huang, X. Peng, D. Mei, M. Li, G. Liu, M. Wu, T. Zhao, B. Huang, *Adv. Mater.* **2021**, *33*, e2103054.

[28] M. Choi, S. H. Lee, Y. Kim, S. B. Kang, J. Shin, M. H. Kwak, K.-Y. Kang, Y.-H. Lee, N. Park, B. Min, *Nature* **2011**, *470*, 369.

[29] N. I. Landy, S. Sajuyigbe, J. J. Mock, D. R. Smith, W. J. Padilla, *Phys. Rev. Lett.* **2008**, *100*, 207402.

[30] F. Costa, A. Monorchio, G. Manara, *IEEE Trans. Antenn. Propag.* **2010**, *58*, 1551.

[31] Yashwanth R. Padooru, Alexander B. Yakovlev, Chandra S. R. Kaipa, Francisco Medina, Francisco Mesa, *Phys. Rev. B* **2011**, *84*, 35108.

[32] D. P. Sheehan, *Entropy* **2012**, *14*, 1915.

[33] N. Lee, T. Kim, J.-S. Lim, I. Chang, H. H. Cho, *ACS Appl. Mater. Interf.* **2019**, *11*, 21250.

[34] H. Wang, P. Kong, W. Cheng, W. Bao, X. Yu, L. Miao, J. Jiang, *Sci. Rep.* **2016**, *6*, 23081.

[35] M. Pan, Y. Huang, Q. Li, H. Luo, H. Zhu, S. Kaur, M. Qiu, *Nano Energy* **2020**, *69*, 104449.

[36] H. Zhu, Q. Li, C. Zheng, Y. Hong, Z. Xu, H. Wang, W. Shen, S. Kaur, P. Ghosh, M. Qiu, *Light Sci. Appl.* **2020**, *9*, 60.

[37] N. Lee, B. Yoon, T. Kim, J.-Y. Bae, J.-S. Lim, I. Chang, H. H. Cho, *ACS Appl. Mater. Interf.* **2020**, *12*, 8862.

[38] T.-H. Ting, K.-H. Wu, J.-S. Hsu, M.-H. Chuang, C.-C. Yang, *J. Chin. Chem. Soc.* **2008**, *55*, 724.

[39] H. Tian, H.-T. Liu, H.-F. Cheng, *Chin. Phys. B* **2014**, *23*, 25201.

[40] N. Engheta, *Science* **2007**, *317*, 1698.

[41] N. Lee, J.-S. Lim, I. Chang, D. Lee, H. H. Cho, *Int. J. Heat Mass Transf.* **2021**, *173*, 121173.

[42] N. Lee, J.-S. Lim, I. Chang, D. Lee, H. H. Cho, *ACS Appl. Mater. Interf.* **2021**, *13*, 43524.

[43] M. I. Skolnik, *Introduction to radar* **1962**.

[44] Dupont, *Dupont Kapton Polyimide Film General Specifications, Bulletin GS-96-7*, http://www.dupont.com/kapton/general/H-38479-4.pdf.

[45] E. Hecht, *Optics*, Addison Wesley San Francisco **2002**.

[46] N. Liu, M. Mesch, T. Weiss, M. Hentschel, H. Giessen, *Nano Lett.* **2010**, *10*, 2342.

[47] T. D. Dao, K. Chen, S. Ishii, A. Ohi, T. Nabatame, M. Kitajima, T. Nagao, *ACS Photon.* **2015**, *2*, 964.

[48] Z. M. Zhang, G. Lefever-Button, F. R. Powell, *Int. J. Thermophys.* **1998**, *19*, 905.

[49] Y. Cengel, *Heat and mass transfer: fundamentals and applications*, McGraw-Hill Higher Education **2014**.

[50] E. H. Sondheimer, *Adv. Phys.* **2001**, *50*, 499.

[51] T. Kim, H. Lee, J.-Y. Bae, T. Kim, J. Cha, D. Jung, H. H. Cho, *IEEE Trans. Aerosp. Electron. Syst.* **2016**, *52*, 2467.